Biosensors and Bioelectronics 140 (2019) 111356

Contents lists available at ScienceDirect

Biosensors and Bioelectronics

journal homepage: www.elsevier.com/locate/bios

Highly sensitive determination of L-tyrosine in pig serum based on ultrathin CuS nanosheets composite electrode

Qin Zhu[a,1], Chu Liu[a,1], Li Zhou[a], Ling Wu[a,b], Kejun Bian[a], Julan Zeng[a], Jianxiu Wang[b], Zemeng Feng[c], Yulong Yin[c], Zhong Cao[a,*]

[a] Collaborative Innovation Center of Micro/nano Bio-sensing and Food Safety Inspection, Hunan Provincial Key Laboratory of Materials Protection for Electric Power and Transportation, School of Chemistry and Biological Engineering, Changsha University of Science and Technology, Changsha, 410114, PR China
[b] College of Chemistry and Chemical Engineering, Central South University, Changsha, 410083, PR China
[c] Institute of Subtropical Agriculture, Chinese Academy of Sciences, Changsha, 410125, PR China

ARTICLE INFO

Keywords:
L-tyrosine
Copper sulfide
Nanosheet
Ultrastructure
Composite electrode
Pig serum

ABSTRACT

Nanometer-sized copper sulfide has remarkable properties such as metal like electrical conductivity and electrocatalytic activity. In this work, ultrathin copper sulfide nanosheets (CuS NS) were synthesized and employed to modify on surface of glassy carbon electrode (GCE) combining with chitosan (CS) and acidified multi-walled carbon nanotubes (F-MWCNTs). Scanning electron microscopy (SEM) and transmission electron microscopy (TEM) showed that the shape of CuS NS was hexagon with side length of 13.33 ± 0.67 nm and thickness of 4.50 ± 0.58 nm. The electrochemical characteristics of different nanocomposite modified electrodes were examined by using cyclic voltammetry (CV) and differential pulse voltammetry (DPV), indicating that the modified electrode of CuS NS-CS/F-MWCNTs/GCE possessed good electrocatalytic activity towards oxidation of L-tyrosine (L-Tyr). Under the optimal condition, the modified electrode exhibited a wide linear response range for L-Tyr (0.08–1.0 μM) with a detection limit of 4.9 nM. No obvious interferences from coexisted two-fold of L-tryptophan and 50-fold of other amino acids could be observed, indicating its relatively good selectivity. The electrode also had good repeatability, reproducibility and stability. Compared with a commercial instrument analytical method, HPLC, the electrode can be successfully applied to the determination of L-Tyr in pig serums with a recovery rate of 95.7%–102.6%, and its test results are in good agreement with that of HPLC, showing its promising application value.

1. Introduction

L-Tyrosine (L-Tyr) is a nutritionally essential amino acid and a vital constituent of proteins (Pradhan et al., 2014; Slominski et al., 2012), which plays an important role in metabolism and growing development of human beings and animals. It was a precursor of neurotransmitters and hormones, which has been found in foods such as fish, soy, eggs, milk, and bananas (Banderet and Lieberman, 1989; Colzato et al., 2014, 2016). However, high levels of L-Tyr have been related to tyrosinemia disease, which was a rare autosomal recessive disorder of L-Tyr metabolism. There was an irreversible damage caused by this disease, especially in case of newborn, including liver failure, painful neurologic crises, rickets, neurological damages and hepatocarcinoma (Scott, 2006). Moreover, the absence of L-Tyr could cause albinism and alkaptonuria (Sueishi et al., 2015). And the content of tyrosine could also affect the nutrition and color of the animals, like pig and goat (Rezaei et al., 2013). Therefore, it is very important to develop a rapid, simple and sensitive method for determination of L-Tyr in the fields of animal nutrition and disease diagnosis.

At present, numerous methods have been used for detection of L-Tyr including spectrophotometry (Hasani et al., 2007), ion-exchange chromatography (Allard et al., 2004), high performance liquid chromatography (HPLC) (Mu et al., 2012), liquid chromatography-mass spectrometry (LC-MS) (Chaki et al., 2018), capillary electrophoresis (Bayle et al., 2003), and fluorescence spectroscopy (Li et al., 2016), etc. However, these methods were cumbersome, expensive, and complicated to operate, which limited their application. With the advantages of simple operation, low cost, good selectivity, and high sensitivity, electrochemical sensors have seen increased interests for detection of small nitrogen-containing molecules (Cao et al., 2019; Chen et al.,

* Corresponding author.
E-mail address: zhongcao2004@163.com (Z. Cao).
[1] These authors contributed equally to this work.

https://doi.org/10.1016/j.bios.2019.111356
Received 19 February 2019; Received in revised form 23 May 2019; Accepted 26 May 2019
Available online 29 May 2019
0956-5663/

2016; Li et al., 2018; Lv et al., 2016, 2017; Sheng et al., 2018; Tahernejad-Javazmi et al., 2018; Yang et al., 2018; You et al., 2019), in particular for L-Tyr combining with nanomaterials (D'Souza et al., 2016; Madrakian et al., 2014; Wang et al., 2017b; Wei et al., 2018). Remarkably, NiO/carbon nanotubes (CNTs) and (2-(3,4-dihydroxyphenethyl)isoindoline-1,3-dione) modified carbon paste electrode (CPE) was employed for simultaneous determination of captopril, acetaminophen, tyrosine, and hydrochlorothiazide, and the detection limit of Tyr was 1.0 μM (Karimi-Maleh et al., 2017). A multi-walled carbon nanotube (MWCNT) or CNT/TiO_2 modified screen-printed electrode (SPE) were used for electroanalysis of L-Tyr, exhibiting their good electrocatalytic activity and analytical performance towards oxidation of L-Tyr, and the linear range for Tyr in human serum was 0.025–1 mM (Shumyantseva et al., 2018). In addition, by using chitosan (CS) as a fixing agent, an activated glassy carbon electrode (GCE) modified with graphene oxide (GO)-ε-MnO_2 microspheres was constructed for sensitive determination of Tyr in milk and dried blood spot samples, that the detection limit was 8.3 nM (Wang et al., 2017a). Up to now, it is still very interesting to develop highly sensitive electrochemical sensors for the determination of L-Tyr in bioscience fields.

In the construction of electrochemical sensing interfaces, MWCNTs had variable diameters of up to 100 nm and were intertwined with each other, resulting in poor dispersibility and solubility (Chung et al., 2014; Jia et al., 2016). After acid treatment, a large number of carboxyl and hydroxyl functional groups were introduced on MWCNTs, which increased more reactive sites, thereby improving the dispersibility and solubility (Avilés et al., 2009; Cao et al., 2011; Long et al., 2012; Xun et al., 2016; Zhang et al., 2015). As a kind of macromolecule, chitosan (CS) is a non-toxic polysaccharide with biocompatibility, biodegradability, excellent film-forming ability and solubility (Cao et al., 2011; Wu et al., 2014; Zarate-Trivino et al., 2015). Interestingly, copper sulfide (CuS) is an important P-type semiconductor, which has been widely used in photocatalysis and photoelectric conversion like for fabricating a counter electrode of solar cell devices (Ke et al., 2014) and a monolith cathode of Li-ion batteries (Cheng et al., 2014). At present, various synthesis approaches have been developed to build CuS nanomaterials with different sizes and shapes, such as nanowire (Ji et al., 2017), nanoflower (Tian et al., 2011), nanoprism (Hsu et al., 2015), mesoporous nanoshell (Chen et al., 2015), and hollow sphere (Yu et al., 2009), etc. Recently, CuS has been found to show excellent properties including metal like electrical conductivity, which may have important application in electrochemical sensors (Goel et al., 2014; Venkadesh et al., 2017). Through self-assembly, a CuS sol-gel film modified capacitive immunosensor was developed for direct detection of human IgA (Wu et al., 2010). In addition, an electrochemical sensor based on CuS-MWCNT nanocomposite has been fabricated, which could be used for determination of nitrite with good reproducibility and strong anti-interference ability (Zhang et al., 2016). Typically, the nonenzymatic sensor based on CuS nanotube (CuS NTs) for detection of glucose, showing that the conductivity and electrocatalytic performance of the composite electrode can be significantly increased while comparing to that of bare electrode (Qian et al., 2013). However, the electrochemical sensors based on ultrathin metal sulphide nanostructures for the detection of L-Tyr have not been reported so far.

In this work, the ultrathin CuS nanosheets (CuS NS) with thickness of sub-5 nm were synthesized, and then assembled onto the surface of functionalized MWCNTs (denoted as F-MWCNTs) modified glassy carbon electrode (GCE) using chitosan (CS) as a dispersant. The modified electrode showed excellent electrocatalytic oxidation activity to L-Tyr molecule, which was due to the exceptional structure of small dimension for such synthesized CuS nanocrystal. It can also be used for highly sensitive determination of L-Tyr in pig serum samples with a recovery rate of 95.7–102.6%, which is comparable to that of a commercial instrument like HPLC. And the detection limit can reach 4.9 nM. It shows that the CuS NS modified electrode possesses important and promising application value in the fields of animal nutrition and biochemical analysis.

2. Experimental

2.1. Materials

Cuprous chloride (CuCl), oleylamine (OA) and octylamine (OTA) were commercially obtained from Shanghai Aladdin Biochemical Technology Co. Ltd. (China). Multi-walled carbon nanotubes (MWCNTs) were purchased from Nanjing Jicang Nano Technology Co. Ltd. (China). Chitosan (CS) was obtained from Shanghai Boao Biotechnology Co. Ltd. (China). L-tyrosine (L-Tyr), L-histidine (L-His), L-cysteine (L-Cys), L-lysine (L-Lys), L-glutamic acid (L-Glu), L-methionine (L-Met), L-glycine (L-Gly), L-proline (L-Pro), L-valine (L-Val), L-phenylalanine (L-Phe), L-isoleucine (L-Ile), sodium hydroxide, potassium ferrocyanide ($K_4[Fe(CN)_6]$), potassium ferricyanide ($K_3[Fe(CN)_6]$), sodium dihydrogen phosphate, and disodium hydrogen phosphate were obtained from Sinopharm Chemical Reagent Co. Ltd (Shanghai, China). All chemicals used in the experiment were of analytical grade. Ultrapure fresh water with a specific resistance of larger than 18.3 MΩ·cm was used throughout all the experiments.

2.2. Instrumentation

All electrochemical measurements were performed on a CHI–760B workstation (Shanghai Chenhua Instruments Co., China) using a conventional three-electrode system, which consisted of a bare or modified glassy carbon electrode (GCE, 3 mm in diameter) as a working electrode, a platinum wire as a counter electrode and an Ag/AgCl as a reference electrode. The pH values were measured with a REX PHSJ-4A PH Meter (INESA Instrument Co. Ltd., Shanghai, China). Material characterizations of microscope images were obtained on a Nova Nano230 field emission scanning electron microscope (FEI, USA) and a JEM-2100 transmission electron microscope (Nippon Electronics Co. Ltd., Japan). Fourier transform infrared (FTIR) spectra were recorded with a model of Vertex 70 FTIR spectrophotometer (Bruker, Germany). X-ray photoelectron spectra (XPS) were obtained on a Thermo Scientific K-Alpha + spectrometer (USA). Routine quantification of L-Tyr in each pig serum sample was performed via Agilent 1260 high performance liquid chromatograph (USA) which was used for comparative test.

2.3. Preparation of functionalized MWCNTs

Functionalized MWCNTs (denoted as F-MWCNTs) were prepared as follows: Firstly, pristine MWCNTs were dissolved in a mixture of concentrated sulfuric acid and nitric acid (v/v, 3:1) following by ultrasonic agitation for about 4 h and refluxing at 120 °C for 2 h. Subsequently, the produced MWCNTs were washed and collected through centrifugation till a neutral pH was achieved. Finally, the acid-treated MWCNTs with carboxylic acid groups were dried at 60 °C in a vacuum drying oven.

2.4. Preparation of CuS nanosheets

According to a method (Du et al., 2012), CuS nanosheets (CuS NS) were prepared as follows: First, adding 0.3 g of cuprous chloride (CuCl) into the mixture of 10 mL oleylamine (OA) and 10 mL octylamine (OTA), the produced paste liquid was heated to 100 °C for removing water and oxygen through vacuum magnetic stirring for 30 min. Then, the paste liquid was heated and maintained at 130 °C for 4 h until the solution became transparent. Subsequently, the dispersion mixture of 0.29 g sulfur powder dissolved in 5.0 mL OA and 5.0 mL OTA was quickly injected into the transparent solution, heated and maintained at 95 °C for 18 h. Finally, the solution was cooled to room temperature, centrifuged and washed for three times with a large amount of absolute ethanol, the precipitate of black powder was obtained, then dried, sealed and stored in a refrigerator at 4 °C prior to use.

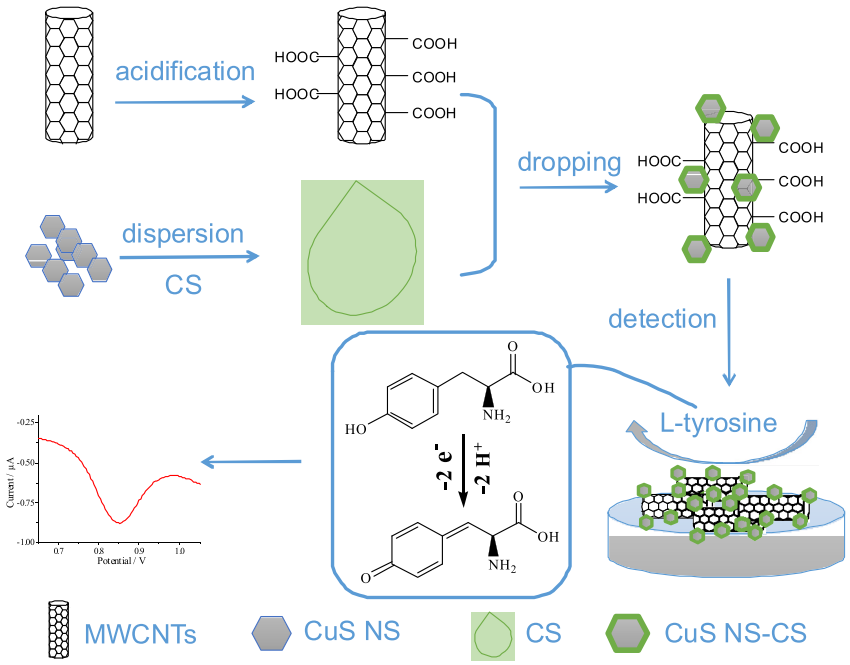

Fig. 1. Schematic illustration of the construction for the composite electrode of CuS NS-CS/F-MWCNTs/GCE and its detection principle for L-Tyr.

2.5. Fabrication of the composite electrodes

The prepared F-MWCNTs (1.0 mg/mL) were dispersed in absolute ethanol. And the prepared CuS nanosheets (5.0 mg/mL) were dispersed in absolute ethanol containing 0.2% chitosan (CS) to form a mixture of CuS NS-CS. Both dispersions were sonicated for 10 min, and then stored in a refrigerator at 4 °C prior to use.

A schematic illustration for the construction process of the composite electrode is shown in Fig. 1. Firstly, the bare glassy carbon electrode (GCE) was sequentially polished with 1.0, 0.3, and 0.05 μm alumina slurry on chamois leather, followed by rinsing with pure water, ethanol and pure water, respectively. The dispersions of F-MWCNTs (4 μL) first and then CuS NS-CS (4 μL) were dropped onto the surface of cleaned GCE. After drying at room temperature, the electrode of CuS NS-CS/F-MWCNTs/GCE can be thus obtained (Fig. 1). For comparison, other modified electrodes like F-MWCNTs/GCE and CuS NS-CS/GCE were fabricated according to the above-mentioned procedure.

2.6. Pretreatment and measurement of pig serum samples

Pig serums were provided by the Institute of Subtropical Agriculture, Chinese Academy of Sciences (Changsha, China). All pig serums were come from healthy Duroc × Landrace × Yorkshire pigs with about 25 kg weighed. Each pig serum was collected in 10 mL centrifuge tube with heparin sodium through neck piercing, and the collected serum was stored at 4 °C for an hour and centrifuged at 3000 rpm for 10 min, then transferring supernatant to a new centrifuge tube and keeping at −20 °C prior to use. Five different pig serum samples were diluted 100 times with phosphate buffer solution (PBS, pH = 7.0). The content of L-Tyr in each pig serum was detected by using the modified electrode and a commercial instrument of HPLC at the meantime.

The procedure for HPLC analysis on tyrosine in the serum was performed as follows: Each pig serum of 200 μL was mixed with 600 μL of acetonitrile, centrifuged at 13200 rpm for 5 min, and the resultant supernatant was subjected to chromatographic analysis. The column of a BCH C18 column (2.1 × 100 mm, 1.7 μm, Waters, USA) was used, and the column temperature was controlled at 50 °C. Using the mobile phase consisting of acetonitrile and H_2O (3:1, V/V), the chromatographic separation was carried out at a flow rate of 1.0 μL/min.

3. Results and discussion

3.1. Characterization of composite materials

The surface morphologies of different composite modified electrodes like F-MWCNTs/GCE (a), CuS NS-CS/GCE (b), and CuS NS-CS/F-MWCNTs/GCE (c) were characterized by using field emission scanning electron microscopy (FESEM) in Fig. 2a–c. It can be seen that the acidified carbon nanotubes are well dispersed and adhered on the surface of glassy carbon electrode (Fig. 2a). Furthermore, the high resolution morphologies of MWCNTs (d) and F-MWCNTs (e) were obtained by using transmission electron microscopy (TEM) for comparison. As shown in Fig. 2d and e, the carbon nanotubes (Fig. 2d) have been opened or split after the acid treatment (Fig. 2e), which could enhance their dispersion and solubility, being beneficial for the electron conduction performance. Fig. 2b is a SEM image of the mixture of the synthesized copper sulfide nanosheets and chitosan (CS), it can be seen that the CuS nanoparticles are well mixed with chitosan and well dispersed on the surface of GCE, and also the particles are of sheet structure which are stacked together. The morphology of the composite of CuS NS-CS/F-MWCNTs is shown in Fig. 2c, and it can be observed that the F-MWCNTs and the CuS nanosheets are well combined to form a kind of nanocomposite, as there are a lot of carboxyl terminals produced on the edge of opened carbon nanotubes after acidification, and some week hydrogen bonds between the functional carboxyl groups and sulfur atom of CuS may be formed. Thus, it plays an important role for current signal amplification in the electrochemical reaction process.

There are further evidences from the chemical characterization of FTIR and XPS data, which could prove the presence of the surface functional groups formed after the acid treatment. As shown in FTIR spectra of MWCNTs (upper) and F-MWCNTs (lower) in Fig. S1 in the Supporting Information, the wide and large peak at 3000–3500 cm^{-1} (lower curve of Fig. S1) is assigned to the characteristic peak of –OH group, which indicates that the –OH group is introduced on the surface of the MWCNTs after the acid treatment. It is clear that the peaks at 1628 cm^{-1} in the spectra of F-MWCNT are increased largely, which are

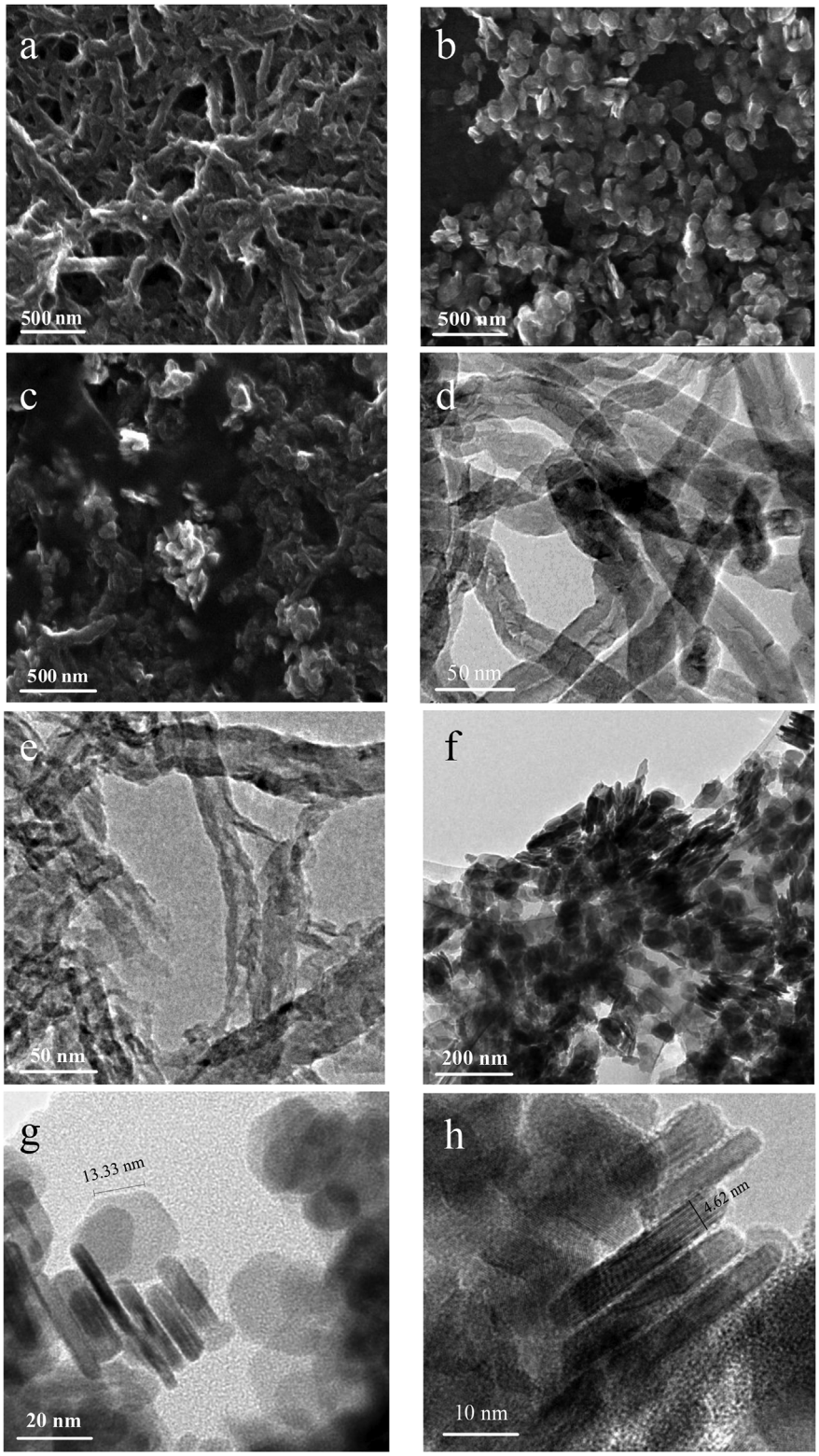

Fig. 2. Characterization of nano materials by using field emission scanning electron microscopy (FESEM) and transmission electron microscopy (TEM). FESEM images for surface morphologies of different composite modified electrodes including F-MWCNTs/GCE (a), CuS NS-CS/GCE (b), and CuS NS-CS/F-MWCNTs/GCE (c). TEM images of MWCNTs (d), F-MWCNTs (e), and ultrathin CuS nanosheets (f) with the amplified morphologies (g, h).

caused by the C═O stretching vibration in the carboxyl groups. Moreover, 1100–1200 cm^{-1} appears at the C–O bond stretching vibration. These results demonstrate that a certain amount of carboxyl groups and hydroxyl groups are generated on the surface of F-MWCNTs. On the other hand, XPS spectra of C1s for MWCNTs (upper) and F-MWCNTs (lower) are shown in Fig. S2 in the Supporting Information. The C1s peaks of C1s A and C1s B located at 283.88 and 284.56 eV correspond to the sp^2 and sp^3 hybrid structures in the carbon nanotube structure, respectively. The binding energy 288.73eV of C1s C is assigned to C═O. It further proved that the carboxyl groups are produced

on the acidified MWCNTs. And the C peak of the sp^2 is weakened, and the C peak of the sp^3 is enhanced, which is caused by the acidification treatment of producing oxygen-containing groups on the MWCNTs. Also, the peaks of Cu and S atoms have been observed in corresponding energy dispersive system (EDS) analysis (Fig. S3 in the Supporting Information), and the reason for the high Al peak is that the aluminum sheet is used as substrate in the experiment.

The ultrastructure of the synthesized CuS nanosheets can be well observed from the images of transmission electron microscope (Fig. 2f–h), which have been directly proved that the sheet CuS particles are distinctly stacked, layer by layer (Fig. 2f). From the amplified morphologies (Fig. 2g and h), it can be clearly observed that there are different orientation like lying and standing for CuS nanosheets, indicating that the shape of the individual CuS nanosheet is hexagon with a side length of 13.33 ± 0.67 nm (n = 9) (Fig. 2g) and a thickness of 4.50 ± 0.58 nm (n = 9) (Fig. 2h). Moreover, the corresponding distance between adjacent nanosheets can be determined to about 0.2–0.5 nm (Fig. 2h). Therefore, the synthesized CuS nanosheet is a kind of nanocrystal with the ultramicrostructure.

3.2. Electrochemical characterization

Electrochemical methods of cyclic voltammetry (CV) and differential pulse voltammetry (DPV) were employed to validate the different composite electrodes. Fig. 3A shows the CV plots of the different

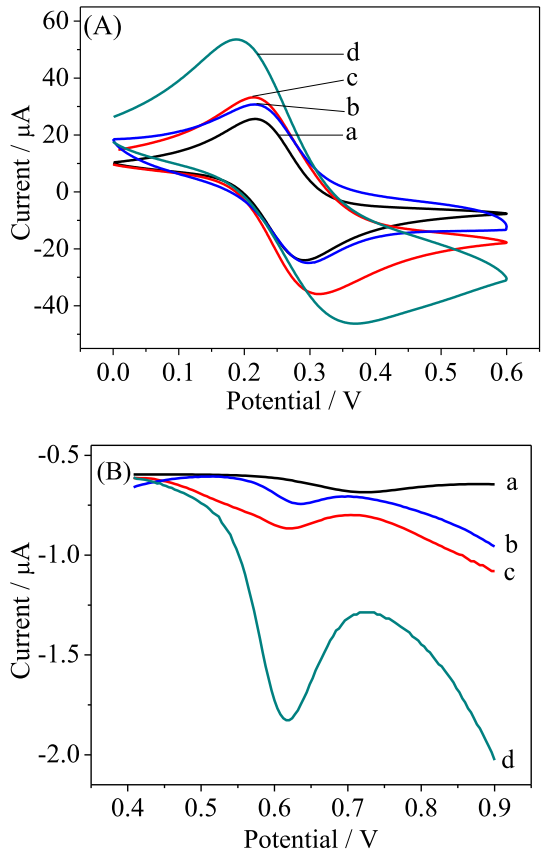

Fig. 3. Electrochemical characteristics curves of different electrodes with cyclic voltammetry (CV) and differential pulse voltammetry (DPV). (A) Typical CV plots of different modified electrodes including bare GCE (a), F-MWCNTs/GCE (b), CuS NS-CS/GCE (c), and CuS NS-CS/F-MWCNTs/GCE (d) in 0.10 mol/L phosphate buffer solution (PBS, pH = 7.0) containing 1.0 mM $K_3[Fe(CN)_6]$/$K_4[Fe(CN)_6]$. (B) Typical DPV plots of the oxidation of L-Tyr at different modified electrodes including bare GCE (a), F-MWCNTs/GCE (b), CuS NS-CS/GCE (c), and CuS NS-CS/F-MWCNTs/GCE (d) in PBS (0.10 M, pH = 7.0) containing 40.0 μM L-Tyr.

electrodes including bare GCE (a), F-MWCNTs/GCE (b), CuS NS-CS/GCE (c), and CuS NS-CS/F-MWCNTs/GCE (d) in a 0.10 M phosphate buffer solution (PBS, pH 7.0) containing 1.0 mM $K_3[Fe(CN)_6]/K_4[Fe(CN)_6]$. As can be seen from Fig. 3A, there is a pair of distinctly reversible redox peaks at the bare electrode which is due to $[Fe(CN)_6]^{3-/4-}$. When the bare GCE is modified with F-MWCNTs and CuS NS-CS respectively, the corresponding peak currents are increased that obey an order of bare GCE (eg. I_{pc} = 13.98 μA) < F-MWCNTs (eg. I_{pc} = 26.99 μA) < CuS NS-CS (eg. I_{pc} = 39.80 μA). After the F-MWCNTs/GCE is modified with CuS NS-CS, a pair of well-defined redox peaks are observed at E_{pa} = 0.368 V and E_{pc} = 0.188 V, with the peak currents of I_{pa} = −37.69 μA and I_{pc} = 48.15 μA, respectively. Thus, the extremely large increased peak currents are obtained by the composite of CuS NS-CS/F-MWCNTs at the surface of the electrode. It can be seen that the F-MWCNTs can slightly enhance the conductivity of the electrode, and the CuS NS-CS can strongly enhance the same and also the corresponding cathodic peak potential shift negatively from 0.218 V to 0.188 V (ΔE = 0.030 V), which means it may further improve the ability of electron transferring rate and electrocatalytic oxidation activity ascribing to its exceptionally small dimensions and the resultant quantum size effects.

The electrochemical oxidation behaviors of L-tyrosine (L-Tyr) at different modified electrodes including bare GCE (a), F-MWCNTs/GCE (b), CuS NS-CS/GCE (c), and CuS NS-CS/F-MWCNTs/GCE (d) were examined by using differential pulse voltammetry in PBS (0.10 M, pH = 7.0) containing 40.0 μM L-Tyr (Fig. 3B). Seen from Fig. 3B, the DPV oxidation peak current of CuS NS-CS/F-MWCNTs/GCE is extremely larger than that of the F-MWCNTs/GCE, CuS NS-CS/GCE and also the bare electrode, and the oxidation peak potential is also negatively shifted, from 0.720 V to 0.632 V, then to 0.620 V and 0.612 V, respectively, indicating that there is a quite strong electrocatalytic activity for L-Tyr at the surface of the composite electrode of CuS NS-CS/F-MWCNTs/GCE. Therefore, the composite electrode can be used for highly sensitive detection of L-Tyr due to its excellent electric conductivity and electrocatalytic oxidation ability.

3.3. Effect of pH

Acidity of solution is an important factor affecting the oxidation reaction of L-Tyr at the electrode surface. The anodic peak currents of L-Tyr (40.0 μM) at the CuS NS-CS/F-MWCNTs/GCE in the pH range of 4.0–8.0 have been investigated by DPV (Fig. S4A in the Supporting Information). It was clear that the anodic peak currents gradually increased as improving pH from 4.0 to 7.0. However, the peak currents gradually decreased with further increasing pH from 7.0 to 8.0. When the pH was equal to 7.0, the peak currents reached a maximum. Therefore, the value of 7.0 was selected as the optimum pH for detecting L-Tyr.

The relationship between the L-Tyr anodic peak potential and pH value has also been examined (Fig. S4B in the Supporting Information). Seen from Fig. S4B, the anodic peak potentials of L-Tyr at the electrode decreased linearly with increasing the pH value, suggesting that the deprotonation is involved in the oxidation process. The corresponding regression equation can be fitted as E_{pa} = 1.04054–0.05781 pH, and the correlation coefficient (r) is 0.9835. According to Nernst equation: $E_p = E_0 + 0.05916\ (m/n)\ pH$, where, m is the number of protons transferred, n is the number of electrons transferred, it can be deduced that m/n = 0.9772, i.e. $m \approx n$. Therefore, the oxidation reaction with an equivalent transfer of electrons and protons for L-Tyr molecule was occurred at the interface of the modified electrode.

3.4. Effect of scan rates

The oxidation peak currents and potentials of CuS NS-CS/F-MWCNTs/GCE varied with different scan rates were examined by CV in 0.10 M PBS (pH = 7.0) containing 40.0 μM L-Tyr (Fig. S5A in the

Supporting Information). It can be seen that the oxidation peak currents increase linearly with the scan rates increased (Fig. S5B in the Supporting Information), and the linear regression equation is fitted as $I_{pa} = -1.0014v - 1.00734$, $r = 0.9987$, indicating that the oxidation of *L*-Tyr at the surface of modified electrode is an adsorption-controlled process.

As shown in Fig. S5C in the Supporting Information, the oxidation peak potentials for L-Tyr increase linearly with increasing the logarithm of the scan rates. The corresponding regression equation can be expressed as: $E_{pa} = 0.06166 \lg v + 0.60323$ ($r = 0.9918$). According to the Laviron equation (Laviron, 1979):

$$E_{pa} = E^{0'} - \frac{2.303RT}{\alpha nF}\lg\frac{RTk^0}{\alpha nF} + \frac{2.303RT}{\alpha nF}\lg v \quad (1)$$

where, E_{pa} is the oxidation peak potential; $E^{0'}$ is the formula potential; α is the electron transfer coefficient; n is the electron transfer number; T is the temperature; R is the molar gas constant; F is the Faraday constant; k^0 is the standard out-of-phase electron transfer rate constant; v is the scan rate, and then $\alpha n = 0.9591$ can be obtained while compared with the above regression equation. Since α is equal to 0.4–0.6 for an irreversible electrode reaction, $n \approx 2$ can be calculated correspondingly. Therefore, it is concluded that the number of electrons transferred during the oxidation process of L-Tyr at the CuS NS-CS/F-MWCNTs/GCE is about 2, and then the number of protons transferred is 2, that is $m = 2$. The detailed reaction mechanism of L-Tyr or L-2-Amino-3-(4-hydroxyphenyl)propanoic acid (**1**) at the electrode surface is illustrated in Fig. 4. During the oxidation process, the phenolic hydroxyl group on the benzene ring of L-Tyr loses an electron to produce a positively charged free radical (**2**), then undergoes deprotonation to form a intermediate (**3**) and intramolecular rearrangement to become a 4-free radical-2-amino-3-(4-oxocyclohexa- 2,5-dienyl) propanoic acid (**4**). By further oxidizing, one electron is lost to produce a positive ion (**5**), which is deprotonated to form the final phenylhydrazine (**6**).

3.5. Linear range and detection limit

Under the optimal condition, the analytical performance of the presented CuS NS-CS/F-MWCNTs/GCE was evaluated by determination of L-Tyr with a series of different concentrations in 0.10 M PBS (pH = 7.0). Fig. 5A shows the DPV responses for the different concentrations of L-Tyr at the modified electrode. It is observed that the oxidation peak currents of the electrode increase with the increasing L-Tyr concentrations from 0.08 μM to 1.0 μM. As shown in an inset plot (Fig. 5B), the electrode exhibits a linear relationship between the oxidation peak currents for target molecule of L-Tyr and its corresponding concentrations in the range of 0.08–1.0 μM. The corresponding regression equation can be expressed as $I_{pa} = -1.64962\,C + 0.09255$ ($r = 0.9961$), and the lower limit of detection is calculated to 0.0049 μM according to three times of signal to noise (S/N = 3). In addition, the comparison of the modified electrode with other amperometric electrodes previously reported elsewhere (Chekin et al., 2016; D'Souza et al., 2016; Madrakian et al., 2014; Rahman et al., 2015; Wang et al., 2017a,b; Zheng et al., 2018; Zhu et al., 2014; Zou et al., 2019) has been examined in detail (see Table S1 in the Supporting Information), indicating that the modified electrode possesses relatively good linear range and low limit for the detection of L-Tyr.

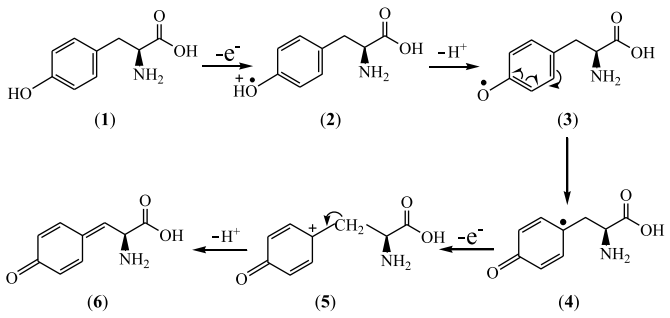

Fig. 4. Proposed oxidation mechanism of L-Tyr at CuS NS-CS/F-MWCNTs/GCE.

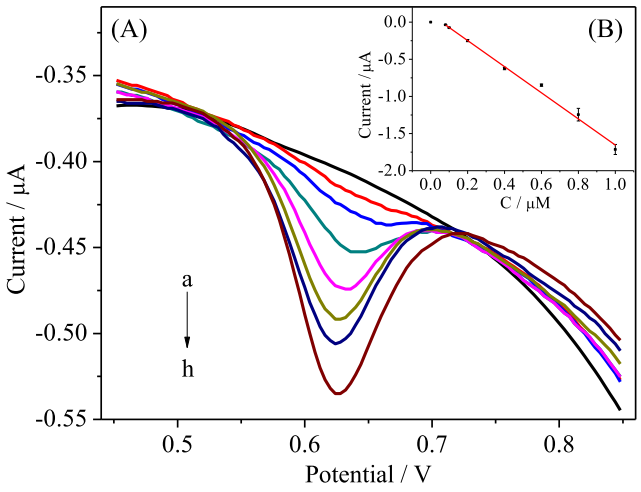

Fig. 5. (A) DPV response curves of CuS NS-CS/F-MWCNTs/GCE in 0.10 M PBS (pH = 7.0) containing different concentrations of L-Tyr. (B) Inset is a plot of linear relationship between the oxidation peak currents and the concentrations of L-Tyr. a→h: 0, 0.08, 0.1, 0.2, 0.4, 0.6, 0.8, 1.0 μM.

3.6. Repeatability, reproducibility and stability

In order to examine the repeatability of CuS NS-CS/F-MWCNTs/GCE, six experiments with the same electrode were repeated for test in the presence of 0.5 μM L-Tyr. The results show that the relative standard deviation (RSD) of the oxidation peak currents is 3.50%, indicating that the modified electrode has good repeatability. To evaluate the reproducibility, six different modified electrodes were fabricated under the same condition independently. And the values of RSD are 2.75% for 0.5 μM L-Tyr by using the six electrodes, indicating the electrodes' reliability of the fabrication procedure. Additionally, the stability of the electrode was also examined, and the current response was measured every day and continuously recorded for 10 d, then the response signal retained 93.54% of the initial value for 0.5 μM of L-Tyr, demonstrating its long lifetime and stable sensitivity.

3.7. Interference studies

In order to investigate the anti-interference performance, the fabricated CuS NS-CS/F-MWCNTs/GCE has been used for detection of 0.5 μM of L-Tyr in the presence of various amino acids (Fig. S6 in the Supporting Information). As shown in Fig. S6A in the Supporting Information, almost not any interferences coming from 50-fold of those amino acids including L-arginine (L-Arg), L-isoleucine (L-Ile), L-aspartic acid (L-Asp), L-phenylalanine (L-Phe), L-histidine (L-His), L-methionine (L-Met), L-lysine (L-Lys), L-alanine (L-Ala), L-proline (L-Pro), L-glycine (L-Gly), L-glutamic acid (L-Glu), L-valine (L-Val), L-threonine (L-Thr) and L-leucine (L-Leu) are observed due to their corresponding currents changed below 5% while coexisting. In addition, there is no interference from L-tryptophan (L-Trp) with coexisting concentration of below two-fold of L-Tyr (0.5 μM), i.e., less than 1.0 μM (Fig. S6B in the Supporting Information). Therefore, it is found that the fabricated electrode has relatively good selectivity for L-Tyr.

3.8. Real samples analysis

To validate practical applicability of the CuS NS-CS/F-MWCNTs/GCE, the fabricated electrode was applied to the detection of L-Tyr in

Table 1
Determination of L-Tyr in pig serums and corresponding recovery.

Sample	HPLC [a] (μM)	Modified electrode [b] (μM)	RE (%)	Spiked (μM)	Found [b] (μM)	Recovery rate (%)	RSD (%)
Serum 1	0.4169	0.4045	−2.97	0.4000	0.8271	102.6	4.2
Serum 2	0.4157	0.4060	−2.33	0.4000	0.8245	102.2	2.1
Serum 3	0.3408	0.3393	−0.44	0.5000	0.8350	98.8	4.7
Serum 4	0.4246	0.4195	−1.20	0.6000	0.9998	95.7	3.2
Serum 5	0.5033	0.5066	+0.66	0.7000	1.1775	96.3	3.6

Note:
[a] The data was measured by using the Agilent 1260 HPLC.
[b] The data was measured by using the modified electrode (n = 5).

pig serums in comparison with a commercial instrument such as the Agilent 1260 HPLC. As shown in Table 1, the detection results of the modified electrode are in consistent with those obtained by using the HPLC method. Moreover, the recovery rate of L-Tyr in the pig serums with the modified electrode is ranged from 95.7% to 102.6%, and the corresponding RSD is less than 5.0% (n = 5), demonstrating that this method can be used for the quantitative determination of L-Tyr in pig serums with good accuracy and precision.

4. Conclusions

Based on a new kind of synthesized hexagonal ultrathin copper sulfide nanosheets (CuS NS) with thickness of 4.50 ± 0.58 nm, a novel composite electrode combining with acidified multi-walled carbon nanotubes and chitosan has been well constructed in the present work. The sensor exhibits strong electron conductivity and electrocatalytic performance toward L-tyrosine (L-Tyr), one of nutritionally essential amino acids by its exceptional nanostructure of small dimension. Almost no interferences from other common amino acids can be observed. Imperfectly, there still is a risk of interference coming from L-tryptophan (L-Trp) when its coexisting concentration is higher than two-fold of L-Tyr. It is worth to notice that the modified electrode has excellent repeatability, reproducibility, stability and a low detection limit of 4.9 nM. Therefore, the present method possesses important application prospect for the detection of L-Tyr in the fields of animal nutrition and life science in the future.

Declaration of interests

The authors declare that they have no known competing financial interests or personal relationships that could have appeared to influence the work reported in this paper.

CRediT authorship contribution statement

Qin Zhu: Investigation, Writing - original draft. **Chu Liu:** Investigation, Writing - original draft. **Li Zhou:** Data curation. **Ling Wu:** Formal analysis. **Kejun Bian:** Formal analysis. **Julan Zeng:** Formal analysis. **Jianxiu Wang:** Formal analysis. **Zemeng Feng:** Validation. **Yulong Yin:** Validation. **Zhong Cao:** Conceptualization, Funding acquisition, Writing - review & editing, Supervision.

Acknowledgements

This work was financially supported by the projects of National Natural Science Foundation of China (Nos. 31527803, 21545010, and 21275022).

Appendix A. Supplementary data

Supplementary data to this article can be found online at https://doi.org/10.1016/j.bios.2019.111356.

References

Allard, P., Cowell, L.D., Zytkovicz, T.H., Korson, M.S., Ampola, M.G., 2004. Clin. Biochem. 37, 857–862.
Avilés, F., Cauich-Rodríguez, J.V., Moo-Tah, L., May-Pat, A., Vargas-Coronado, R., 2009. Carbon 47, 2970–2975.
Banderet, L.E., Lieberman, H.R., 1989. Brain Res. Bull. 22, 759–762.
Bayle, C., Siri, N., Poinsot, V., Treilhou, M., Caussé, E., Couderc, F., 2003. J. Chromatogr. A 1013, 123–130.
Cao, Z., Zhao, Y.T., Dai, Y.M., Long, S., Guo, X.C., Yang, R.H., 2011. Sens. Lett. 9, 1985–1989.
Cao, Z., Li, W.F., Liu, C., Peng, Y.Y., Huang, Y., Xiao, Z.L., 2019. Chinese J. Anal. Chem. 47, 229–236.
Chaki, M., Sánchez-Calvo, B., Carreras, A., Valderrama, R., Begara-Morales, J.C., Corpas, F.J., Barroso, J.B., 2018. Identification of tyrosine and nitrotyrosine with a mixed-mode solid-phase extraction cleanup followed by liquid chromatography-electrospray time-of-flight mass spectrometry in plants. In: Mengel, A., Lindermayr, C. (Eds.), Nitric Oxide: Methods and Protocols. Humana Press, New York, pp. 161–169.
Chekin, F., Bagheri, S., 2016. Russ. J. Electrochem. 52, 174–180.
Chen, F., Hong, H., Goel, S., Graves, S., Orbay, H., Ehlerding, E., Shi, S., Theuer, C., Nickles, R., Cai, W., 2015. ACS Nano 9, 3926–3934.
Chen, D., Cao, Z., Liu, F., Wu, L., Xun, Y., He, J., Xiao, Z., 2016. Chinese J. Anal. Chem. 44, 1593–1599.
Cheng, J., Pan, Y., Zhu, J., Li, Z., Pan, J., Ma, Z., 2014. J. Power Sources 257, 192–197.
Chung, S.H., Manthiram, A., 2014. J. Phys. Chem. Lett. 5, 1978–1983.
Colzato, L.S., Jongkees, B.J., Sellaro, R., Wildenberg, W., Hommel, B., 2014. Neuropsychologia 62, 398–402.
Colzato, L.S., Steenbergen, L., Sellaro, R., Stock, A., Arning, L., Beste, C., 2016. Cortex 82, 217–224.
Du, Y., Yin, Z., Zhu, J., Huang, X., Wu, X., Zeng, Z., Yan, Q., Zhang, H., 2012. Nat. Commun. 3, 1177.
D'Souza, O.J., Mascarenhas, R.J., Satpati, A.K., Aiman, L.V., Mekhalif, Z., 2016. Ionics 22, 405–414.
Goel, S., Chen, F., Cai, W., 2014. Small 10, 631–645.
Hasani, M., Moloudi, M., Emami, F., 2007. Anal. Biochem. 370, 68–76.
Hsu, S.W., Ngo, C., Bryks, W., Tao, A.R., 2015. Chem. Mater. 27, 4957–4963.
Ji, L., Zhu, L., Wang, J., Chen, Z., 2017. Electrochim. Acta 252, 516–522.
Jia, G., Hu, Y., Qian, Q., Yao, Y., Zhang, S., Li, Z., Zou, Z., 2016. ACS Appl. Mater. Interfaces 8, 14527–14534.
Karimi-Maleh, H., Ganjali, M.R., Norouzi, P., Bananezhad, A., 2017. Mater. Sci. Eng. C 73, 472–477.
Ke, W., Fang, G., Lei, H., Qin, P., Tao, H., Zeng, W., Wang, J., Zhao, X., 2014. J. Power Sources 248, 809–815.
Laviron, E., 1979. J. Electroanal. Chem. Interfacial Electrochem. 101, 19–28.
Li, Y., Cai, N., Wang, M., Na, W., Shi, F., Su, X., 2016. RSC Adv. 6, 33197–33204.
Li, Y., Zhu, Q., Xiao, Z., Lű, C., Feng, Z., Yin, Y., Cao, Z., 2018. Chem. J. Chinese Univ. 39, 636–644.
Long, S., Tian, Y.F., Cao, Z., He, J.L., Luo, D.M., 2012. Sens. Actuators, B 166–167, 223–230.
Lv, C.Z., Chen, D., Cao, Z., Liu, F., Cao, X.M., He, J.L., Zhao, W.Y., 2016. Int. J. Electrochem. Sci. 11, 10107–10122.
Lv, C.Z., Xun, Y., Cao, Z., Xie, J.L., Li, D., Liu, G., Yu, L., Feng, Z.M., Yin, Y.L., Tan, S.Z., 2017. Food Anal. Methods 10, 2252–2261.
Madrakian, T., Haghshenas, E., Afkhami, A., 2014. Sens. Actuators, B 193, 451–460.
Mu, S., Li, Y., Tang, A.-G., Xiao, L.-D., Ren, Y.-P., 2012. Clin. Chim. Acta 413, 973–977.
Pradhan, T., Jung, H.S., Jang, J.H., Kim, T.W., Kang, C., Kim, J.S., 2014. Chem. Soc. Rev. 43, 4684–4713.
Qian, L., Mao, J., Tian, X., Yuan, H., Xiao, D., 2013. Sens. Actuators, B 176, 952–959.
Rahman, M.M., Lopa, N.S., Kim, K., Lee, J., 2015. J. Electroanal. Chem. 754, 87–93.
Rezaei, R., Wang, W., Wu, Z., Dai, Z., Wang, J., Wu, G., 2013. J. Anim. Sci. Biotechnol. 4, 7.
Scott, C.R., 2006. Am. J. Med. Genet. Part C Semin. Med. Genet. 142C, 121–126.
Sheng, Y.Y., You, Y., Cao, Z., Liu, L., Wu, H.C., 2018. Analyst 143, 2411–2415.
Shumyantseva, V., Bulko, T., Kuzikov, A., Masamrekh, R., Archakov, A., 2018. Amino Acids 50, 823–829.
Slominski, A., Zmijewski, M.A., Pawelek, J., 2012. Pigm. Cell Melan. Res. 25, 14–27.
Sueishi, Y., Takemoto, T., 2015. Bioorg. Med. Chem. Lett 25, 1808–1810.
Tahernejad-Javazmi, F., Shabani-Nooshabadi, M., Karimi-Maleh, H., 2018. Talanta 176, 208–213.
Tian, Q., Tang, M., Sun, Y., Zou, R., Chen, Z., Zhu, M., Yang, S., Wang, J., Wang, J., Hu, J., 2011. Adv. Mater. 23, 3542–3547.
Venkadesh, A., Radhakrishnan, S., Mathiyarasu, J., 2017. Electrochim. Acta 246, 544–552.
Wang, S., Zhai, H., Chen, Z., Wang, H., Tan, X., Sun, G., Zhou, Q., 2017a. J. Electrochem. Soc. 164, B758–B766.
Wang, Y., Xiong, C., Qu, H., Chen, W., Ma, A., Zheng, L., 2017b. J. Electroanal. Chem. 799, 321–326.
Wei, Z., Yang, Y., Xiao, X., Zhang, W., Wang, J., 2018. Sens. Actuators, B 255, 895–906.
Wu, Z., Cao, Z., Zeng, J.L., Zhang, L., Chu, X., Shen, G.L., Yu, R.Q., 2010. Anal. Sci. 26, 1001–1006.
Wu, L., Cao, Z., Song, T.M., Song, C., Xie, J.L., He, J.L., Xiao, Z.L., 2014. Chinese J. Anal. Chem. 42, 1656–1660.
Xun, Y., Cao, Z., Song, T.M., Lv, C.Z., Liu, F., He, J., Yang, R., 2016. Chem. J. Chinese

Univ. 37, 835–843.
Yang, J., Zhang, Y.Y., Liu, C., Li, J.X., Xiao, Z.L., Li, D., Zhang, L., Cao, Z., 2018. Chem. J. Chinese Univ. 39, 2386–2394.
You, Y., Zhou, K., Guo, B., Liu, Q., Cao, Z., Liu, L., Wu, H.C., 2019. ACS Sens. 4, 774–779.
Yu, X.L., Wang, Y., Chan, H.L.W., Cao, C.B., 2009. Microporous Mesoporous Mater. 118, 423–426.
Zarate-Trivino, D.G., Prokhorov, E., Luna-Bárcenas, G., Mendez-Nonell, J., González-Campos, J.B., Elizalde-Pena, E., Mota-Morales, J.D., Santiago-Jacinto, P., Terrones, M., Gomez-Salazar, S., Nuno-Donlucas, S.M., Sanchez, I.C., 2015. Mater. Chem. Phys. 155, 252–261.
Zhang, M.L., Huang, D.K., Cao, Z., Liu, Y., He, J.L., Xiong, J.F., Feng, Z.M., Yin, Y.L., 2015. LWT-Food Sci. Tech. 64, 663–670.
Zhang, S., Li, B., Sheng, Q., Zheng, J., 2016. J. Electroanal. Chem. 769, 118–123.
Zheng, W., Zhao, M., Liu, W., Yu, S., Niu, L., Li, G., Li, H., Liu, W., 2018. J. Electroanal. Chem. 813, 75–82.
Zhu, S., Zhang, J., Zhao, X., Wang, H., Xu, G., You, J., 2014. Microchim. Acta 181, 445–451.
Zou, J., Mao, D., Wee, A.T.S., Jiang, J., 2019. Appl. Surf. Sci. 467, 608–618.